

PAPER • OPEN ACCESS

Anomalous delocalization of resonant states in graphene & the vacancy magnetic moment

To cite this article: Mirko Leccese and Rocco Martinazzo 2023 *Electron. Struct.* **5** 024010

View the [article online](#) for updates and enhancements.

You may also like

- [Phonons from density-functional perturbation theory using the all-electron full-potential linearized augmented plane-wave method FLEUR](#)
Christian-Roman Gerhorst, Alexander Neukirchen, Daniel A Klüppelberg et al.
- [Assessment of localized and randomized algorithms for electronic structure](#)
Jonathan E Moussa and Andrew D Baczewski
- [Assessing the correlated electronic structure of lanthanum nickelates](#)
Frank Lechermann

Electronic Structure



PAPER

Anomalous delocalization of resonant states in graphene & the vacancy magnetic moment

OPEN ACCESS

RECEIVED

23 February 2023

REVISED

12 May 2023

ACCEPTED FOR PUBLICATION

6 June 2023

PUBLISHED

30 June 2023

Original Content from this work may be used under the terms of the [Creative Commons Attribution 4.0 licence](https://creativecommons.org/licenses/by/4.0/).

Any further distribution of this work must maintain attribution to the author(s) and the title of the work, journal citation and DOI.

Mirko Leccese¹ and Rocco Martinazzo^{1,2,*} ¹ Department of Chemistry, Università degli Studi di Milano, Via Golgi 19, 20133 Milano, Italy² Istituto di Scienze e Tecnologie Chimiche 'Giulio Natta', CNR, Via Golgi 19, 20133 Milan, Italy

* Author to whom any correspondence should be addressed.

E-mail: rocco.martinazzo@unimi.it**Keywords:** local magnetic moment, carbon atom vacancy, graphene, resonant state, slab-supercell, inverse participation ratio, hybrid functionals

Abstract

Carbon atom vacancies in graphene give rise to a local magnetic moment of $\sigma + \pi$ origin, whose magnitude is yet uncertain and debated. Partial quenching of π magnetism has been ubiquitously reported in periodic *first principles* calculations, with magnetic moments scattered in the range 1.0–2.0 μ_B , slowly converging to the lower or the upper end, depending on how the diluted limit is approached. By contrast, (ensemble) density functional theory calculations on cluster models neatly converge to the value of 2 μ_B when increasing the system size. This stunning discrepancy has sparked a debate about the role of defect–defect interactions and self-doping, and about the importance of the self-interaction-error in the density-functional-theory description of the vacancy-induced states. Here, we settle this puzzle by showing that the problem has a fundamental, mono-electronic origin which is related to the special (periodic) arrangement of defects that results when using the slab-supercell approach. Specifically, we report the existence of resonant states that are *anomalously* delocalized over the lattice and that make the π midgap band *unphysically* dispersive, hence prone to self-doping and quenching of the π magnetism. Hybrid functionals fix the problem by widening the gap between the spin-resolved π midgap bands, without reducing their artificial widths. As a consequence, while reconciling the magnetic moment with expectations, they predict a spin-splitting which is one order of magnitude larger than found in experiments.

1. Introduction

Defects in graphene such as monovalent ad-species or missing carbon atoms—commonly referred to as ‘ p_z vacancies’—play important roles in charge transport, in magnetism and in the chemistry of graphene, since they induce semi-localized ‘midgap’ states which are known to decay slowly (as $1/r$) from the defect position [1–3]. These resonant states host itinerant electrons, act as strong scatterers determining graphene conductivity at both zero and finite carrier densities [4–8], and provide spin-half semi-local magnetic moments which are detectable by magnetometry experiments [9, 10] and bias graphene chemical reactivity towards specific lattice positions [11–13].

Carbon atom vacancies play a special role in this respect since, besides the above ‘midgap’ state, they present additional dangling bonds in the σ skeleton originating from the removal of a C atom. In the bare vacancy a structural (Jahn–Teller) distortion occurs [14–17] and leaves a lonely σ electron which is free to couple with the above mentioned π one. As a result, the ground state of the bare vacancy in large cluster models is predicted to be a (planar) ‘triplet’, although a (non-planar) ‘singlet’ with one spin flipped (only ~ 0.2 eV higher in energy) can be accessed if ripples in the graphene sheet or interaction with a substrate are taken into account [18]. Periodic calculations do predict a planar, high-spin configuration but fail in reproducing the ‘expected’ value of the magnetic moment [15–20].

It is well known that periodic calculations can be plagued by spurious interactions between periodic images that determine the displacement and the broadening of the defect-related bands, hence causing

self-doping and partial quenching of the magnetization. However, several works have reported a *reduction* of the local magnetic moments upon increasing the cell size thereby suggesting a complete quenching of the π magnetism in the diluted limit [19]. Others suggest an increase of the magnetic moment towards $\sim 1.5 \mu_B$ when decreasing the defect concentrations [14–18, 20], and one of them predicts the ‘expected’ limit of $2 \mu_B$ when the limit of an isolated vacancy is carefully approached [21]. As a matter of fact, the computed values of the magnetic moment scatter in the range 1.0–1.7 μ_B , and slowly converge to 1 μ_B or 2 μ_B , depending on how the limit of an isolated vacancy is realized. By contrast, calculations based on clusters models show that the magnetic moment increases with cluster size, clearly tending to the expected value of $2 \mu_B$ [20]. Therefore, calculations including periodicity produce the opposite result of cluster based simulations.

This puzzling issue has been recently addressed by employing computationally expensive hybrid functionals in periodic calculations, with the gratifying reward of a reasonable value of the magnetic moment, smoothly converging to $2 \mu_B$ when increasing the supercell size [22, 23]. The immediate conclusion of these studies is that exact exchange is crucial for the correct description of the vacancy magnetic moment: hybrid functionals partially correct the self-interaction error (SIE) that notoriously plagues local (LDA) and semi-local (GGA) functionals and that can seriously affect the degree of electron localization/delocalization, hence the magnetization. This seems to be a definite answer to the long-debated issue of the magnetic moment of a C-atom vacancy in graphene, but it is quite unsatisfactory from a theoretical point of view. Indeed, this ‘magnetic-moment problem’ does not involve at all the σ electron³, rather resides in the semilocalized (*not even normalizable*) ‘midgap’ state where e - e interactions hardly play a significant role. All the more that GGA calculations for other p_Z defects, e.g. H atoms, predict the ‘correct’ π moment, with precisely the same defect-induced π structure underneath [13].

Here, motivated by these puzzling issues we reinforce some observations made long ago by one of the present authors (R M) about the existence of anomalously delocalized states in defective graphene that could hamper the correct calculation of the magnetic moment in a periodic setting [18, 24]. We do this by scrutinizing the localization properties of the midgap state wavefunctions at both the tight-binding (TB) and the *first principles* theory levels (section 3), after providing a comprehensive theoretical frame for their discussion (section 2) which should clarify the anomalous character of the delocalization. By relating the anomalous delocalization of the states to the *dispersion* of the π midgap band we provide evidence for a spurious self-doping of the band, hence for an *unphysical* quenching of the magnetization. As we shall show below, the problem is not limited to the C atom vacancy, although it affects the vacancy more than other p_Z defects.

2. Theory

In this section we present some background material which is necessary to identify as *anomalous* the behaviour of the midgap state in a periodic calculation (at least in some regions of the supercell Brillouin zone, SBZ). We start by providing some analytical results about the expected spatial properties of the resonance induced by a p_Z vacancy in graphene, and then we show why—at the tight binding level with nearest-neighbors hoppings only—*fully* delocalized states appear that contrast with the $1/r$ decaying states expected for a vacancy. The delocalized solutions are inherited from the pristine system (they are ‘robust’ against some disorder) and, as will be shown numerically in section 3, they survive at higher level of theory and provide a mechanism for self-doping and for the quenching of the π magnetization.

2.1. Isolated p_Z defect

The most complete, yet analytical, description of the zero-mode state induced by a p_Z vacancy in graphene is provided by the non-interacting Anderson model [25] for a simple adsorbed species that covalently binds to one of the graphene lattice sites [4, 6]⁴. The limit of a true C-atom vacancy can then be realized by strengthening the adatom-lattice chemical bond up to the extent that the bonding/antibonding pair of molecular orbitals describing the bond separates out from the lattice states (the so-called unitary limit). The ad-species is described by a single level at energy ε_{ad} (e.g. the $1s$ level of a H atom) which hybridizes with a carbon atom of the lattice. If we place the latter at the origin of the lattice, the total Hamiltonian reads as

$$H = H_{latt} + H_{ad} \quad (1)$$

³ This is hosted in a well localized state featuring a strong Coulomb repulsion (~ 2.5 eV) that prevents double occupation despite the fact it is located well below the Fermi level (~ 0.7 eV).

⁴ See also [13] for a detailed description of the model and of the relevant results.

where

$$H_{\text{latt}} = -t \sum_{\sigma} \sum_{\langle i,j \rangle} c_{i,\sigma}^{\dagger} c_{j,\sigma} \quad (2)$$

is the TB lattice Hamiltonian with nearest-neighbors hoppings and

$$H_{\text{ad}} = \sum_{\sigma} \epsilon_{\text{ad}} d_{\sigma}^{\dagger} d_{\sigma} + W \sum_{\sigma} \left(c_{0,\sigma}^{\dagger} d_{\sigma} + d_{\sigma}^{\dagger} c_{0,\sigma} \right). \quad (3)$$

Here, W is the hybridization energy, d_{σ}^{\dagger} (d_{σ}) creates (destroys) an electron with spin σ in the adatom energy level, $c_{i,\sigma}^{\dagger}$ ($c_{i,\sigma}$) does the same for the lattice site i and t is the hopping energy for the nearest-neighbors pairs $\langle i,j \rangle$. We are interested in the Green's operator⁵ $G(\lambda)$ of the one-electron Hamiltonian, which can be obtained upon partitioning the one-electron space into a primary subspace (the lattice) and the remainder [26]. Its projection onto the lattice—i.e. $PG(\lambda)P$, P being the projector onto the primary subspace—takes the form $PG(\lambda)P = (\lambda - H_{\text{eff}})^{-1} \equiv G_{\text{eff}}(\lambda)$ where H_{eff} is an effective, energy-dependent Hamiltonian implicitly accounting for the dynamics in the adatom level. The latter reads as $H_{\text{eff}} = H_{\text{latt}} + V(\lambda)$ with the local scattering potential defined by

$$V(\lambda) = W^2 \sum_{\sigma} \frac{|\chi_{0,\sigma}\rangle\langle\chi_{0,\sigma}|}{\lambda - \epsilon_{\text{ad}}}$$

where $|\chi_{0,\sigma}\rangle$ is a p_Z spin-orbital at the defective site. The sought for effective Green function can be obtained from the T matrix [27], $T(\lambda) := V + VG_{\text{eff}}(\lambda)V$, since the corresponding Lippmann–Schwinger equation $T(\lambda) = V + VG^0(\lambda)T(\lambda)$ (where G^0 is the Green's operator of the unperturbed lattice) is solved by

$$T(\lambda) = t(\lambda) \sum_{\sigma} |\chi_{0,\sigma}\rangle\langle\chi_{0,\sigma}| \quad t(\lambda) = \frac{W^2}{\lambda - \epsilon_{\text{ad}} - W^2 g_{00}^0(\lambda)} \quad (4)$$

when the potential takes a separable form. Here, $g_{00}^0(\lambda)$ is the on-site Green's function of the unperturbed lattice,

$$g_{00}^0(\epsilon) = \langle 0\sigma | G^0(\lambda) | 0\sigma \rangle \approx -\frac{\epsilon}{\epsilon_c^2} \ln \left(\left| \frac{\epsilon_c}{\epsilon} - 1 \right| \right) - i\pi \rho^0(\epsilon),$$

$\rho^0(\epsilon) \approx \frac{|\epsilon|}{\epsilon_c^2} \Theta(\epsilon_c - |\epsilon|)$ is the density of states per C atom per spin channel and ϵ_c is an energy cutoff that determines the bandwidth, $\epsilon_c \approx \hbar v_F d_{\text{CC}}^{-1}$, where $d_{\text{CC}} \approx 1.42 \text{ \AA}$ is the C–C bond length⁶. Because of the linear density of states, the real part of the on-site Green's function features a vertical cusp at zero energy that has a huge impact on the defect-induced states. Indeed, it makes the position of the resonance defined by equation (4), i.e. the lowest energy solution of the equation

$$\epsilon - \epsilon_{\text{ad}} - W^2 \Re g_{00}^0(\epsilon) = 0,$$

rather insensitive to the hybridization energy W and always very close to $\epsilon = 0$. This feature gives an 'universal' character to the defect problem, meaning that it does not depend on the details of the defect originating the p_Z vacancy in the lattice.

We are interested in the spatial properties of such resonance, i.e. in the scattered component $|\psi_{\epsilon}^{\text{scatt}}\rangle$ of the scattering state $|\psi_{\epsilon+}\rangle$,

$$|\psi_{\epsilon+}\rangle = |\psi_{\epsilon}^0\rangle + |\psi_{\epsilon}^{\text{scatt}}\rangle = |\psi_{\epsilon}^0\rangle + G^0(\epsilon)T(\epsilon)|\psi_{\epsilon}^0\rangle$$

where $|\psi_{\epsilon}^0\rangle$ is an eigenstate of the unperturbed lattice with energy ϵ . Clearly,

$$\psi_{\epsilon}^{\text{scatt}}(\mathbf{r}) \propto t(\epsilon)G^0(\mathbf{r}, 0|\epsilon)$$

where $G^0(\mathbf{r}, 0|\epsilon) = \langle \mathbf{r}\sigma | G^0(\epsilon) | 0\sigma \rangle$ is the Green function of the unperturbed lattice at \mathbf{r} for the adatom sitting on the site at the origin $\mathbf{0}$ (which we take to be of A type in the following). This quantity has been considered

⁵ As usual, λ is understood to be $\lambda = \epsilon + i\eta$, where ϵ is a real energy and $\eta \rightarrow 0^+$.

⁶ Upon matching $\rho^0(\epsilon)$ to the known low-energy expression for the density of states in graphene one obtains $k_c = \epsilon_c/\hbar v_F = 2\sqrt{2\pi/3}\sqrt{3}d_{\text{CC}}^{-1} \approx 2d_{\text{CC}}^{-1}$ or $\epsilon_c = t\sqrt{\pi\sqrt{3}} \approx 6 \text{ eV}$.

by several authors for different reasons—from STM imaging [28] to RKKY interactions in graphene [29–31]—and can be obtained numerically as Fourier transform of the (simpler) Green’s function in k -space, namely from

$$G_{XA}^0(\mathbf{r}, 0|\epsilon) = \frac{1}{\Omega_{\text{BZ}}} \int_{\text{BZ}} d^2\mathbf{k} e^{i\mathbf{k}\mathbf{r}} G_{XA}^0(\mathbf{k}|\epsilon)$$

where $X = A, B$ depending on whether \mathbf{r} is a lattice position in the A or B sublattice (\mathcal{A} and \mathcal{B} , respectively, in the following). Here, the integral runs over the graphene Brillouin zone (BZ) and Ω_{BZ} is its area. At the low energies of interest for the defect-induced resonance, the above expression can be integrated analytically in the linear band approximation with negligible error for not too small distances ($r > d_{\text{CC}}$). The result is

$$G_{AA}^0(\mathbf{r}, 0|\epsilon) = -i \frac{A_c}{2} \frac{|\epsilon| \cos(\mathbf{K}\mathbf{r})}{\hbar^2 v_F^2} H_0^\pm \left(\frac{|\epsilon|r}{\hbar v_F} \right) \quad \text{for } \mathbf{r} \in \mathcal{A} \tag{5}$$

$$G_{BA}^0(\mathbf{r}, 0|\epsilon) = +i \frac{A_c}{2} \frac{\epsilon \sin(\mathbf{K}\mathbf{r} + \theta)}{\hbar^2 v_F^2} H_1^\pm \left(\frac{|\epsilon|r}{\hbar v_F} \right) \quad \text{for } \mathbf{r} \in \mathcal{B} \tag{6}$$

where H_l^\pm are Hankel functions of the first and second kind (for positive and negative energies, respectively) of order l , A_c is the area of the graphene unit cell and θ is the angle between \mathbf{r} and vector \mathbf{K} . The latter locates a K corner in the BZ and can be given as $2\pi\mathbf{K} = \Omega_{\text{BZ}}\boldsymbol{\delta} \wedge \hat{\mathbf{n}}$, where $\boldsymbol{\delta}$ is the position of the B site relative to the A one in the (arbitrarily) chosen unit cell, and $\hat{\mathbf{n}}$ is the surface normal. Thus, the scattering resonance turns out to have the expected threefold symmetry, with maxima along the armchair directions. It further presents the celebrated $1/r$ decay in an intermediate distance range $d_{\text{CC}} < r \ll \hbar v_F/|\epsilon|$, that can be effectively rather wide at the energies of interest ($\epsilon \rightarrow 0$). Indeed, upon replacing the Hankel’s functions in equations (5) and (6) with their low-argument expansion one obtains the approximate expressions

$$G_{AA}^0(\mathbf{r}, 0|\epsilon) \approx \frac{A_c}{\pi} \frac{\epsilon r}{\hbar v_F} \frac{\cos(\mathbf{K}\mathbf{r})}{\hbar v_F} \left[\ln \left(\frac{|\epsilon|r}{2\hbar v_F} \right) + \gamma \right] \quad \text{for } \mathbf{r} \in \mathcal{A} \tag{7}$$

$$G_{BA}^0(\mathbf{r}, 0|\epsilon) \approx \frac{A_c}{\pi} \frac{\sin(\mathbf{K}\mathbf{r} + \theta)}{\hbar v_F} \quad \text{for } \mathbf{r} \in \mathcal{B} \tag{8}$$

(where $\gamma \approx 0.577$ is the Euler–Mascheroni constant) featuring a $1/r$ decay of G^0 on the majority sublattice (\mathcal{B}) and a much smaller magnitude on the minority one (\mathcal{A}), vanishing for $\epsilon \rightarrow 0$.⁷ Such algebraic decay of the wavefunction was first predicted [1, 2, 32–34] and experimentally observed [3] for carbon atom vacancies and more recently investigated for hydrogen atoms [35]. The above equations provide a full spatial description of the π midgap state, which is valid at any distance from the defect position but the smallest ones (i.e. for $r > d_{\text{CC}}$), which however are irrelevant for the present discussion.

2.2. Periodic arrangement of p_Z defects

Next we consider the case—which is rather common when it comes to modeling with *first principles* means—where the p_Z defect is investigated in a periodic setting with a sufficiently large supercell that minimizes any electronic/structural interaction between the defect and its periodic image. We consider again a tight binding model with next-neighbors hoppings only and show that, irrespective of the supercell shape and size there exist regions in the superlattice Brillouin zone where the zero energy modes are anomalous, i.e. they fully delocalize over the lattice *without* decaying as $1/r$ away from the defect positions, as it happens for the isolated defect. These anomalous states do not disperse at the simple tight binding level of theory but do it in the presence of inhomogeneities in the lattice, thereby affecting the correct occupation of k -states in the Brillouin zone and the net induced magnetic moment.

We start observing that, at the above mentioned tight binding level, one of the two linearly independent states that are found at the K point of pristine graphene is also an exact zero-energy solution for the lattice with a p_Z vacancy (the same happens at the K' point). To this end we re-write the lattice Hamiltonian of the unperturbed system, equation (2), by explicitly showing its bipartite nature

$$H_{\text{latt}} = -t \sum_{\sigma} \sum_{\mathbf{R}, i} a_{\mathbf{R}, \sigma}^\dagger b_{\mathbf{R} + \boldsymbol{\delta}_i, \sigma} + \text{c.c.}$$

⁷ For the minority sublattice contribution notice that, with $x = |\epsilon|r/\hbar v_F$, one has $|x \ln x| \leq e^{-1}$ for any $x < 1$.

Here the inner sum runs over the lattice sites, δ_i are the three vectors joining A sites to B sites, and $a_{\mathbf{R},\sigma}$, $b_{\mathbf{R},\sigma}$ are the previous $c_{i,\sigma}$'s annihilation operators, now for an A or a B site, respectively, which is located at \mathbf{R} . The Hamiltonian for the defective lattice with a missing A site at the origin $\mathbf{R} = 0$ then reads as

$$H = H_0 + t \sum_{\sigma} \sum_{i=1}^3 \left(a_{0,\sigma}^{\dagger} b_{\delta_i,\sigma} + b_{\delta_i,\sigma}^{\dagger} a_{0,\sigma} \right). \quad (9)$$

In pristine graphene, the eigenstates at the K (or K') point, because of degeneracy, can be chosen to localize on either sublattice, i.e. to have definite projection of the pseudo-spin along z . Let $|\phi_{K,\sigma}^A\rangle$ and $|\phi_{K,\sigma}^B\rangle$ be such localized states at the K point, respectively for \mathcal{A} and \mathcal{B} . Since they are eigenstates at zero energy we have

$$\sum_{i=1}^3 a_{\mathbf{R},\sigma}^{\dagger} b_{\mathbf{R}+\delta_i,\sigma} |\phi_{K,\sigma}^B\rangle = 0$$

for any lattice vector \mathbf{R} , hence it holds

$$\sum_{i=1}^3 \left(a_{0,\sigma}^{\dagger} b_{\delta_i,\sigma} + b_{\delta_i,\sigma}^{\dagger} a_{0,\sigma} \right) |\phi_{K,\sigma}^B\rangle \equiv 0.$$

This shows that $|\phi_{K,\sigma}^B\rangle$ is also an eigenstate of the defective Hamiltonian H at the same energy.

Next, we observe that this property is not limited to a single vacancy, since similar reasoning applies to an *arbitrary* number of isolated vacancies, provided they are all placed in the A sublattice. In particular, it holds for a *periodic* arrangement of vacancies in large supercells, which is the case of interest when modeling p_z vacancies with a periodic-supercell approach. In such instance, wherever the K and K' points fold to into the SBZ there appear 'preserved' states of the pristine lattice that occupy the majority lattice sites only (as the midgap state ought to) but have an extended character, without decaying as $1/r$ away from the defect. And, by continuity, it is expected on general grounds that this anomalous delocalization of the wavefunction is not limited to the above special points, rather it extends over their neighborhoods in the SBZ. This feature—while not affecting the dispersion of the midgap π band for the (periodized) Hamiltonian of equation (9)⁸—do affect the properties of the corresponding band when, more realistically, $e - h$ symmetry breaks down. For instance, a slight change of the on-site energy has to be expected around a C atom vacancy because of the charge re-distribution that unavoidably occurs at an edge of a graphenic structure, and this suggests that the midgap π band becomes dispersive in those regions of the SBZ where the states are delocalized. In turn, this affects the occupation of the band and the net magnetic moment that it carries. We stress that this dispersion is *unphysical*, meaning that it is a feature of the periodic arrangement of vacancies rather than of the system one would (most probably) like to describe, i.e. an isolated vacancy in graphene.

3. Results

In this section we present some numerical results that support the above interpretation that the dispersion of the π midgap band in a periodic model of vacancies is unphysical (for the purpose of describing an isolated vacancy in the lattice). We start by considering simple TB calculations in which we modelled the vacancy at a very simple level but using relatively large supercells. Then we move to a more realistic description of the C -atom vacancy in graphene by considering density functional theory (DFT) calculations that account for the atomistic details of the defect in the lattice, albeit in a more limited setting.

3.1. Tight-binding

We first investigate the midgap π band in periodic TB Hamiltonians with p_z vacancies, using unperturbed (i.e. homogeneous) on-site energies. We consider for simplicity $n \times n$ superlattices where the anomalies are easily identified since, depending on the superlattice constant n , K and K' fold either to K/K' or to the Γ point of the SBZ. Specifically, when $n \neq 3m$ ($m \in \mathbb{N}$) *non-degenerate* graphene zero-energy modes are expected at both the K and the K' point of the SBZ, since K and K' fold, respectively, into K and K' for $n = 3m + 1$ and into K' and K for $n = 3m + 2$. When $n = 3m$, on the other hand, both K and K' fold into Γ , a Dirac cone survives, and three states are expected at zero energy, two of which (the ones localizing on the majority sites) are necessarily the extended K and K' states of pristine graphene.

⁸ This remains flat all over the SBZ since it is constrained by $e - h$ symmetry to lie at zero energy.

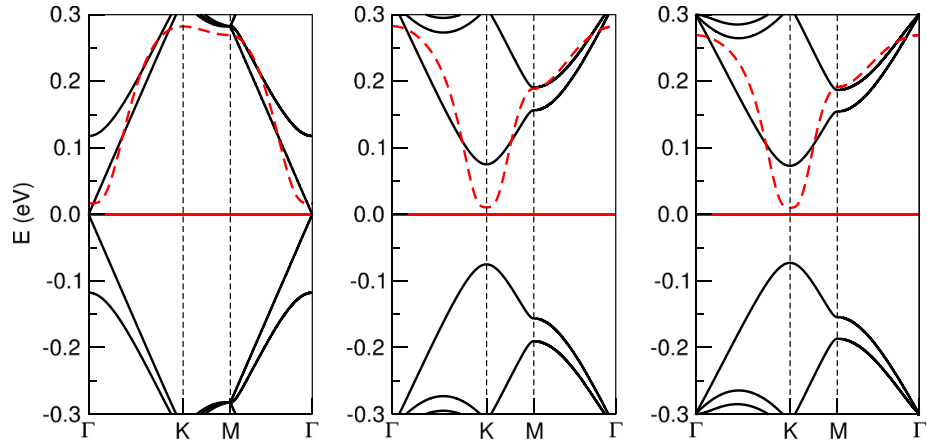


Figure 1. Low energy band structure of $n \times n$ superlattices with one vacancy from tight-binding calculations with $t = 2.7$ eV. $n = 30, 31, 32$ from left to right. Full red lines for the midgap band and dashed red lines for the corresponding inverse participation ratio, see text for details. For $n = 30$ the latter was computed for a state localized on the majority sublattice.

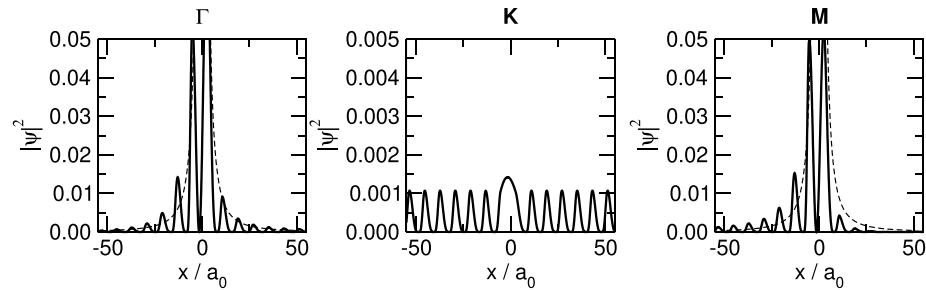


Figure 2. Probability density of the zero-energy modes found at the special points of the superlattice Brillouin zone for $n = 31$, from left to right for Γ, K and M , as indicated. The x axis is placed along one of the three-fold symmetry direction of the defective lattice. Curves are Akima splines interpolating the numerically determined coefficients and dashed lines on the leftmost and on the rightmost panels represent the functions $+1/r^2$.

Figure 1 shows the band-structure of three different superlattices with a (super)lattice constant corresponding to a rather large unit cell, $n = 30, 31, 32$ from left to right. In these calculations the hopping parameter was given the value $t = 2.7$ eV to ease the comparison with the *first principles* results discussed below. In figure 1 the non-dispersive midgap band is plotted in red (full line) and it is accompanied (dashed red line) by its $q = 2$ inverse participation ratio, which is defined as

$$\text{IPR}_q = \sum_i |\psi_i|^{2q} \quad (10)$$

where the sum runs over the lattice sites of the supercell and ψ_i is the amplitude of the zero-energy mode at the i th site. This IPR_q (for $q > 1$) measures the localization of the midgap states in this periodic arrangement of defects. A (normalized) state which is fully delocalized over the lattice gives $\text{IPR}_2 = 1/n^2$, since n^2 is the number of majority sites in a $n \times n$ supercell where the midgap state is known to localize. For a state decaying as $1/r$, on the other hand, the inverse participation ratio takes a larger value, namely $\text{IPR}_2 \approx a/(b + \ln n)^2$ where a and b are constants and the dependence on n follows from the logarithmic divergence of its squared norm. Clearly, the real-space localization properties of the midgap state change across the SBZ and the state does indeed delocalize where the special K and K' points of graphene are found to fold in the SBZ. Figure 2 shows the details of the zero energy wavefunctions for $n = 31$ along one of the three-fold symmetry directions of the vacant lattice, and explicitly proves the existence of delocalized states at special symmetry points of the superlattice Brillouin zone. Similar results are found for $n = 30, 32$, with the only *caveat* that for $n = 30$ three delocalized states are found at Γ as a consequence of the residual degeneracy.

These odd findings are not limited to the above (already large) unit cells, rather persist for any supercell size. This is seen by the IPR_2 computed at the K and the Γ points for several $n \times n$ superlattices of p_z vacancies, which is reported in figure 3. (Please notice that in drawing the figure we set $n \neq 3m$ to free ourselves from the annoying degeneracy problem that prevents the automatic analysis of the zero

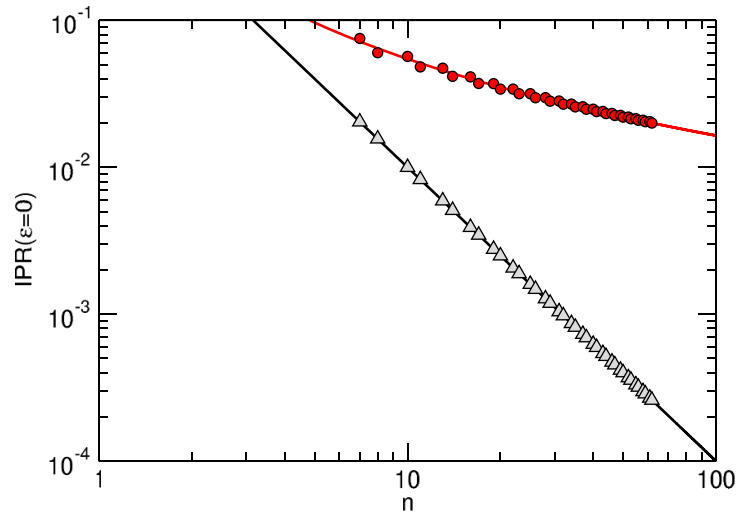


Figure 3. Inverse participation ratio for anomalous (grey triangles) and ordinary (red circles) midgap states in $n \times n$ supercells, as computed at the K and Γ points of the superlattice Brillouin zones, respectively, for n not a multiple of 3. Also shown as full lines, the corresponding theoretical values, namely $\text{IPR}_2 = 1/n^2$ for a fully delocalized state (black curve) and a fit to $\text{IPR}_2 \approx a/(b + \ln n)^2$ appropriate for a state decaying as $1/r$ (red curve).

energy mode.) Also shown in the same figure (full black lines) is the expected behavior of the IPR_2 , that confirms the rather different spatial extensions of the states at the selected special points of the SBZ.

Finally, we illustrate how a varying real-space localization may turn a flat band to be dispersive in the realistic situation where some inhomogeneities in the lattice are present. Figure 4 shows the band structure of a p_z vacancy in a 6×6 cell, as obtained at different levels of theory: tight binding for π states only in the left and middle panels, and *first principles* calculations (to be described below) for a C-atom vacancy in the rightmost panel. For the left panel, tight binding calculations used (as above) a uniform distribution of on-site energies, while for the middle panel we introduced some inhomogeneity in the lattice. Specifically, we shifted the on-site energy of the three lattice sites closest to the defect by 1.0 eV below the value it takes in pristine graphene, in order to mimic the charge redistribution occurring in the σ bands as a consequence of the removal of a C atom. The figure makes clear that the anomalously delocalized zero energy state that appears close to Γ leads, in the presence of inhomogeneities, to a dispersive midgap band which (with the chosen parameters) closely resembles the one found from *first principles* in the atomistic model of the vacancy. At the *first principles* level of theory self-doping necessarily occurs, the Dirac point shifts above the Fermi level and the spin-up and spin-down bands split. Hence, the majority spin channel is only fractionally occupied and the magnetization gets partially quenched, if the comparison is made with the situation of a spin-split but otherwise flat band. We stress that the ‘dispersive region of the SBZ’ shrinks together with the superlattice Brillouin zone when increasing the supercell size *without* disappearing. Hence, in self-consistent calculations, in order to obtain a smooth behavior of the magnetic moment with the system size and to attempt any kind of extrapolation, the larger the supercell is the finer the k mesh should be, as indeed observed in calculations [21].

3.2. First principles calculations

Next, we consider the results of several *first principles* calculations that we performed on different periodic arrangements of C atom vacancies and similar p_z vacancies. In these calculations we used the pseudo-potential DFT implementation available in SIESTA [36, 37], in the generalized gradient approximation provided by the Perdew–Burke–Ernzerhof functional. Separable [38] norm conserving pseudopotentials [39] with partial core corrections [40] were used to replace core electrons, and Kohn–Sham states were represented on a basis of numerical atomic orbitals with compact support. Such an approach allows one to tackle efficiently huge-sized problems, at the expense of a reduced control on the convergence of the one-electron basis. For this reason we used consistently a double- ζ basis set with single polarization orbitals (DZP) but occasionally checked the results with triple- ζ sets and double polarization orbitals (TZ2P), finding negligible differences between the two sets of results. We optimized each structure considering adopting a stringent threshold on the maximum component of the atomic forces ($0.005 \text{ eV \AA}^{-1}$), in conjunction with a large energy cutoff (800 Ry) for the real space integration grid to remove any egg-box effect.

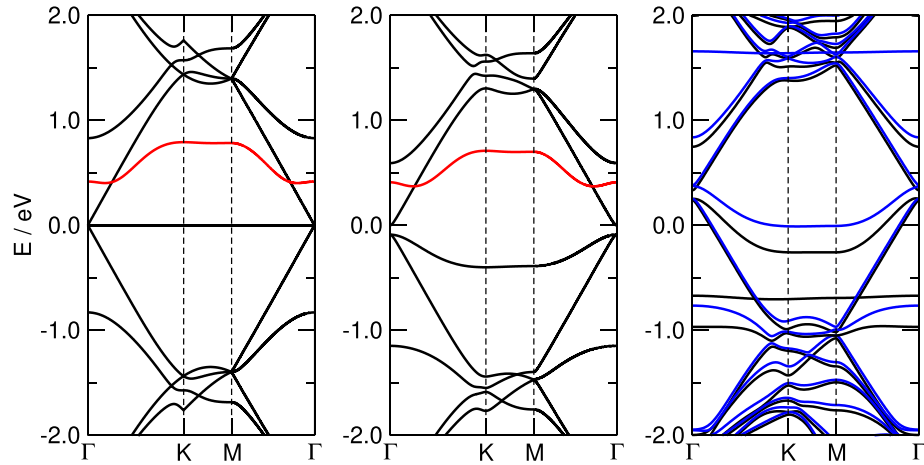


Figure 4. Band structure of a carbon atom vacancy in a 6×6 supercell. Left and middle panels: energy bands (black curves) from tight binding calculations with hopping parameter $t = 2.7$ eV. Red curves are for the inverse participation ratio of the midgap state. Calculations in the middle panel used an energy offset of $\Delta\epsilon = -1.0$ eV for the on-site energy of the three sites closest to the vacancy. Right panel: spin-polarized *first principles* calculations, with black and blue curves for majority spin and minority spin states, respectively. Energies are referenced to the Fermi level.

The detailed structure of a C-atom vacancy is well-known and well described in the literature. Briefly, the removal of a C atom creates a p_z defect responsible for a π resonant state and, at the same time, leaves three dangling orbitals in the σ network. In the D_{3h} point symmetry group of the system the first belongs to the a_2'' symmetry species, while the second span the $a_1' + e'$ irreducible representations. Among the latter, a_1' is lowest in energy since it contains a purely bonding combination of σ orbitals. Hence, the lowest energy configuration of the many-body state is of E'' symmetry and undergoes a standard $E \otimes e$ Jahn–Teller distortion driven by the coupling with in-plane e' vibrations. As a result, a distorted geometry with a ‘pentagonal’ ring and an ‘apical’ carbon atom opposite to it emerges as equilibrium configuration, threefold degenerate. The *vertical* position of the apical C atom determines the preferred spin alignment (through a second order vibronic coupling): in the lowest energy state, this is the high-spin state with the apical C atom in-plane with the graphene sheet. Periodic DFT calculations correctly predict the in-plane arrangement but present a difficult convergence for the monovacancy properties, particularly for the magnetization, as exemplified by table 1 that reports some details for the smallest supercells considered. As we now show, this is due to the anomalous delocalization and the ensuing unphysical dispersion of the midgap-state π band.

Figure 5 reports the low-energy band-structure of some $n \times n$ superlattices with large supercells ($n = 12, 13$ and 14), featuring two dispersive midgap π bands, one for the majority spin species (black) and the other for the minority ones (blue). Their width is large enough to compete with the Coulomb splitting of the band, thereby determining a partial double occupation of the band (hence, a partial quenching of the magnetization) in a way that sensitively depends on the adopted supercell. To show that this is indeed related to the anomalous delocalization discussed above, we computed the IPR_q (for $q = 2$) of the *first-principles* k -wavefunctions describing the midgap state, namely the integrals

$$\text{IPR}_q(\mathbf{k}) = \int_U |\psi_{\mathbf{k}}(\mathbf{r})|^{2q} d^3\mathbf{r} \quad (11)$$

where U is the superlattice unit cell and $\psi_{\mathbf{k}}$ is the (majority-spin) midgap state for k -vector \mathbf{k} . The resulting IPR_2 is reported as red lines in figure 5 and unambiguously shows the presence of delocalized states (small values of the IPR) at the high-symmetry points of the SBZ where the K, K' states of pristine graphene fold to, i.e. the Γ point for $n = 12$ and the K, K' points otherwise. The behavior of the IPR_2 over the SBZ is further shown in figure 6 where it becomes clear that the anomalously delocalized states occupy finite-sized regions of the SBZ (darker area in the color maps), which are much larger than expected on the basis of the band plots alone. Figure 7, on the other hand, provides a real-space picture of the wavefunction delocalization. Specifically, in that figure we compare the anomalously delocalized density at the Γ point of the 12×12 SBZ (left panel) with the ‘normal’ (i.e. $1/r^2$ -decaying) counterpart at the K point of the same SBZ (right panel).

Finally, we notice that the anomalous delocalization and the unphysical dispersion is not limited to the C-atom vacancy, rather occurs for any p_z defect, although its effects on the band filling and the magnetization depends on the details of the defect. This is shown in figure 8 for different p_z defects in the same 12×12 supercell, where the spin-splitting and the band dispersion are seen to depend on the nature of

Table 1. Short ($d_{<}$) and long ($d_{>}$) carbon-carbon distances in the monovacancy and corresponding magnetic moment M from the *first-principles* calculations described in the main text, for different supercell size and k -mesh. For comparison, plane wave calculations for the 6×6 supercell 6×6 with a 6×6 k -mesh result in $d_{<} = 2.007 \text{ \AA}$, $d_{>} = 2.557 \text{ \AA}$, $M = 1.556 \mu_B$.

Supercell	k -mesh	$d_{<} (\text{\AA})$	$d_{>} (\text{\AA})$	$M (\mu_B)$
5×5	4×4	2.128	2.552	1.767
	5×5	2.132	2.553	1.820
	6×6	2.123	2.551	1.720
	8×8	2.127	2.552	1.752
	10×10	2.129	2.552	1.767
	12×12	2.127	2.552	1.751
	24×24	2.130	2.553	1.762
6×6	4×4	2.073	2.551	1.673
	5×5	2.070	2.549	1.667
	6×6	2.067	2.548	1.671
	8×8	2.066	2.548	1.638
	10×10	2.069	2.548	1.654
	12×12	2.069	2.548	1.654
	24×24	2.069	2.549	1.654
7×7	4×4	2.026	2.544	1.637
	5×5	2.012	2.542	1.491
	6×6	2.016	2.543	1.562
	8×8	2.015	2.543	1.547
	10×10	2.016	2.543	1.545
	12×12	2.015	2.542	1.540
	24×24	2.014	2.543	1.535

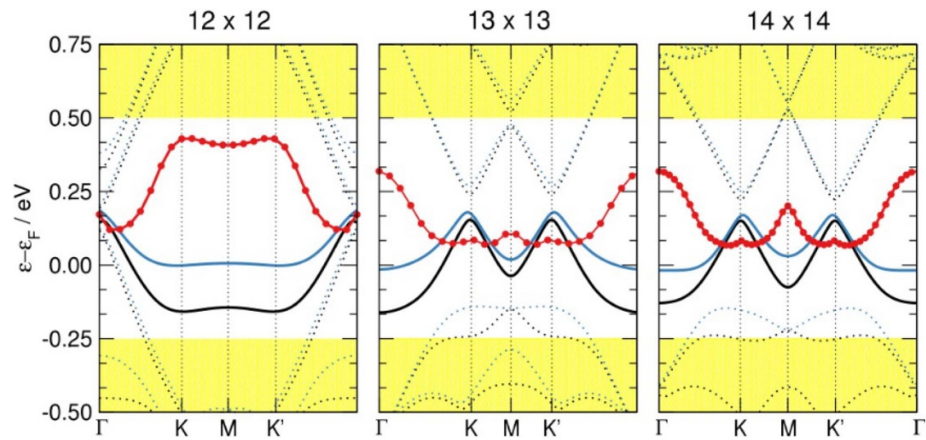


Figure 5. Spin-resolved low energy band structure of the monovacancy in a 12×12 , 13×13 and 14×14 supercell (as indicated). The dispersive midgap band(s) are given as black and blue full lines for the majority and the minority spin components, respectively. Also shown as red lines the inverse participation ratios for the majority-spin midgap state (magnified by 50 times).

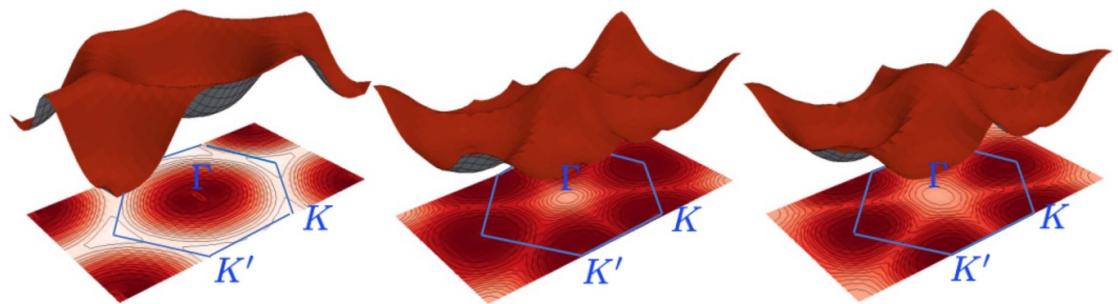


Figure 6. From left to right: behavior of the inverse participation ratio of the majority-spin midgap state in the SBZ of the 12×12 , 13×13 and 14×14 supercells with a C atom vacancy. The SBZ with its high-symmetry points is given by the blue hexagons.

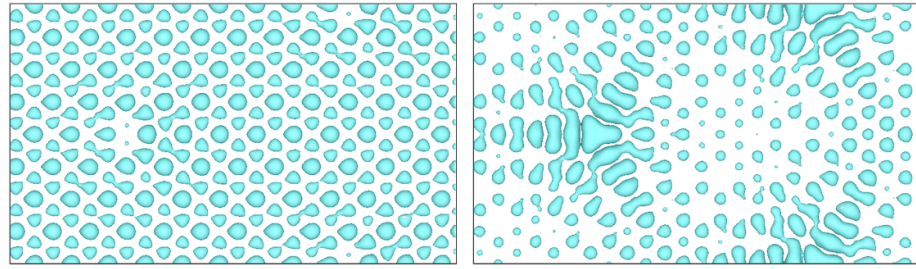


Figure 7. Isocontours of the density $|\psi_{\mathbf{k}}(\mathbf{r})|^2$ for the Γ - and the K -point midgap-state wavefunctions (left and right panel, respectively) in the 12×12 superlattice with a C atom vacancy.

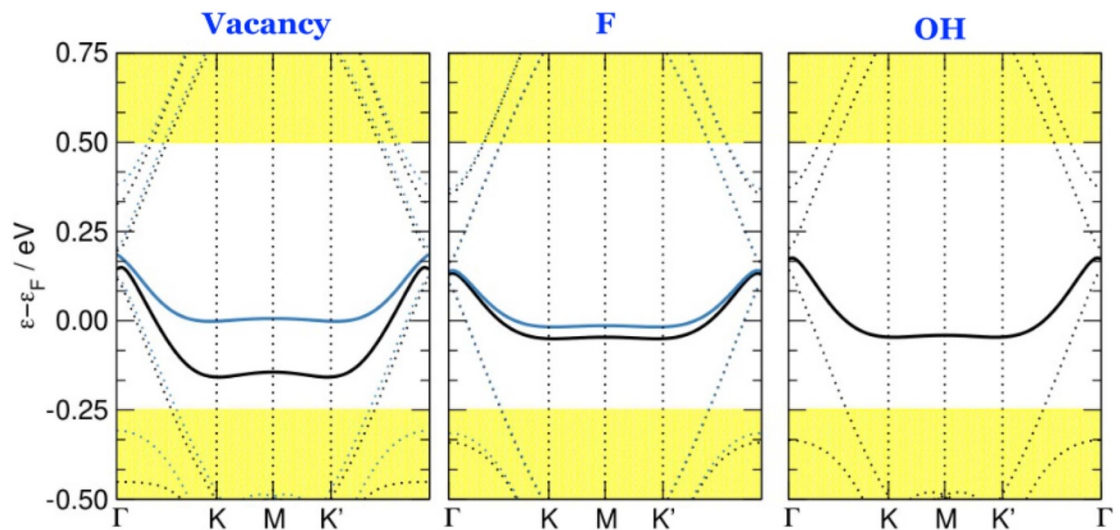


Figure 8. Spin-resolved low energy band structure of the monovacancy and of the F and the OH adsorbates (as indicated), as obtained in a 12×12 supercell. The dispersive midgap band(s) are given as black and blue full lines for the majority and the minority spin components, respectively.

the defect. Hydrogen adatoms (not shown) are rather unique in this respect as they are almost immune to unphysical dispersion. By this we do *not* mean that dispersion of the π midgap band is absent for H adatoms, rather that it is smaller than the spin-splitting of the band, hence irrelevant for its occupation. See, for instance, [35] (figure S17) for the band structure of one H adatom in a large (and skewed) supercell, which features a spin-splitting that is small on an absolute scale but large enough to prevail over band dispersion. The reasons why certain species affect dispersion more than others is yet unknown, but the model tight-binding calculations described in section 3.1 show that the charge inhomogeneities around the defect position are crucial for it. In this respect the electronegativity of the adsorbed atom must play an important role, the closer is this value to that of the C atom the smaller is the charge inhomogeneity, hence the unphysical dispersion.

4. Discussion

The above results unambiguously show that modeling of a C-atom vacancy in graphene in a periodic setting introduces anomalies in its electronic structure that hamper the correct occupation of the bands and determine a partial quenching of the magnetization. Although the difficulties in assessing the magnetic moment with periodic *first principles* calculations have been acknowledged by several authors, they have been attributed to the self-interaction error that plagues local and semi-local functionals and that is known to seriously affect the degree of electron localization/delocalization. In support to this idea some authors have recently employed *hybrid* functionals in periodic calculations to show that they give a magnetic moment that smoothly and rapidly converges to the expected value of $2 \mu_B$ when increasing the supercell size [22, 23].

Similar conclusions can be drawn from Hubbard-corrected DFT calculations⁹. The use of these hybrid functionals that mix some fraction of exact (Hartree–Fock) exchange to the semi-local one—thereby partially correcting the SIE—has led to the immediate conclusion that the SIE is crucial for the correct description of the vacancy and apparently put an end to the long-debated issue of the magnetic properties of an isolated C monovacancy in graphene. The conclusion however is *incorrect*, since it is not physically sound and is inconsistent with experimental findings.

As mentioned in the Introduction, while the SIE argument might be reasonable for a localized resonance characterized by a large Coulomb ‘on-site’ energy, it is untenable for a semilocalized (not normalizable) midgap state whose Coulomb energy hardly exceeds some tens of meV. Indeed, carefully conducted experiments performed on defective graphene samples have demonstrated the presence of spin-split peaks in the local density of states in the neighborhoods of mono-vacancies, with energy separations in the range 20–60 meV [41]. These values agree with the peak separation found by Gonzalez-Herrero *et al* [35] in hydrogenated samples (~ 20 meV) for which (as seen above) the involved resonant state is, for any practical aim, precisely the same as that introduced by a C-atom vacancy. On the other other, the spin-splitting produced by hybrid functionals is one order of magnitude larger—several hundreds of meV, depending on the supercell size—hence unphysical, except maybe in the true diluted limit. It is thanks to the presence of this large splitting that one achieves, with hybrid functionals, the correct occupation of the π midgap band and the smooth convergence of the magnetic moment. The electronic structure, though, remains ‘distorted’ and features yet an unphysically dispersive π midgap band, which is more than 0.5 eV wide for the largest supercell considered so far (16×16 , see figure 3 in [23]). This width is by no means comparable with the ‘intrinsic’ width of the mono-vacancy which is experimentally found of the order $\lesssim 0.05$ eV [41]. Hence, while fixing the problem of filling the midgap band, hybrid functionals do *not* solve the core problem and, by providing a distorted picture of the electronic structure, should be considered with caution when investigating resonance states induced by p_z -vacancies in graphene. To be clear, local and semi-local functionals share similar difficulties (after all, as shown above, these originate from the one-electron part of the problem), but at least they describe the spin splitting reasonably well (figure 5).

5. Summary and conclusions

We have shown that p_z defects in graphene, when periodically arranged, generate a π ‘midgap’ band whose real-space localization properties change across the supercell Brillouin zone, from $1/r$ decaying expected for an isolated vacancy to fully delocalized. The latter states are robust features inherited from the pristine system that spoil the correct description of an isolated vacancy. We emphasize once again how they hamper the calculation of the magnitude of the local magnetic moment of the monovacancy in graphene: in the presence of inhomogeneities the (anomalous) delocalization broadens the defect-induced resonance to such an extent that it spoils its filling. That is, the actual width (Δ) of the resonance is much larger than its intrinsic one (Δ_0)¹⁰ and becomes comparable to (if not larger than) the spin-splitting U determined by the Coulomb repulsion in the resonant state (\sim tens of meV). For the diluted limit of a single vacancy in the lattice we should have $\Delta_0 \ll U$, hence a net π magnetic moment of $1 \mu_B$ which adds to the one provided by the σ state ($1 \mu_B$). However, in the large unit cell limit of a periodic simulation one typically obtains $\Delta_0 \ll \Delta \sim U$, and the magnetization disappears (irrespective of the precise position of the resonance relative to the Fermi level) unless U is artificially increased. The problem is not fixed by improving the theory level—e.g. by adding a fraction of exact exchange to alleviate the self-interaction error that plagues popular density functionals—since it is of mono-electronic origin, as our TB results clearly show.

We have not yet identified any ‘*a priori*’ guideline that can help to predict whether or not a given point defect in graphene is affected by the anomalous dispersion, but on the basis of our findings we are tempted to conclude that *any* kind of p_z defect is prone to anomalous delocalization and should be treated with care. The chemical identity of the defect may affect the size of the artificial dispersion—hence the quenching of the local magnetic moment—however, the correct description of the electronic structure is always prevented by the mere existence of the anomalous delocalization. Even if the latter does not show up in the computed local moment (as it happens for H) it may well affect other properties that more sensitively depend on the spatial features of the resonant state. For these reasons our recommendation is to treat these defects with special

⁹ We thank the anonymous reviewer for providing the results of their DFT + U calculations showing that application of a Hubbard correction of $U = 3.0$ eV to the Carbon p -shell is enough to recover the correct magnetic moment in a 5×5 supercell calculation. However, as discussed below for hybrid functionals, both the spin-splitting and the midgap-band dispersion turn out to be unreasonably large.

¹⁰ According to equation (4), this is proportional to $W^2 \rho^0(\epsilon)$ at the resonant energy $\epsilon = \epsilon_{\text{res}} \approx 0$.

attention, for instance by adopting tailored k -sampling strategies in the slab-supercell approach or, alternatively, by employing embedding techniques.

Data availability statement

The data that support the findings of this study are openly available at the following URL/DOI: https://doi.org/10.13130/RD_UNIMI/EIMQRQ [42].

ORCID iD

Rocco Martinazzo  <https://orcid.org/0000-0002-1077-251X>

References

- [1] Pereira V M, Guinea F, Lopes dos Santos J M B, Peres N M R and Castro Neto A H 2006 *Phys. Rev. Lett.* **96** 036801
- [2] Pereira V M, Lopes dos Santos J M B and Castro Neto A H 2008 *Phys. Rev. B* **77** 115109
- [3] Ugeda M M, Brihuega I, Guinea F and Gómez-Rodríguez J M 2010 *Phys. Rev. Lett.* **104** 096804
- [4] Robinson J P, Schomerus H, Oroszlány L and Fal'ko V I 2008 *Phys. Rev. Lett.* **101** 196803
- [5] Castro Neto A H, Guinea F, Peres N M R, Novoselov K S and Geim A K 2009 *Rev. Mod. Phys.* **81** 109–62
- [6] Wehling T O, Yuan S, Lichtenstein A I, Geim A K and Katsnelson M I 2010 *Phys. Rev. Lett.* **105** 056802
- [7] Peres N M R 2010 *Rev. Mod. Phys.* **82** 2673–700
- [8] Ferreira A, Viana-Gomes J, Nilsson J, Mucciolo E R, Peres N M R and Castro Neto A H 2011 *Phys. Rev. B* **83** 165402
- [9] Nair R R, Sepioni M, Tsai I L, Lehtinen O, Keinonen J, Krasheninnikov A V, Thomson T, Geim A K and Grigorieva I V 2012 *Nat. Phys.* **8** 199–202
- [10] Nair R, Tsai I L, Sepioni M, Lehtinen O, Keinonen J, Krasheninnikov A, Castro Neto A, Katsnelson M, Geim A and Grigorieva I 2013 *Nat. Commun.* **4** 2010
- [11] Hornekaer L, Rauls E, Xu W, Šljivančanin Ž, Otero R, Stensgaard I, Lægsgaard E, Hammer B and Besenbacher F 2006 *Phys. Rev. Lett.* **97** 186102
- [12] Casolo S, Løvrik O M, Martinazzo R and Tantardini G F 2009 *J. Chem. Phys.* **130** 054704
- [13] Bonfanti M, Achilli S and Martinazzo R 2018 *J. Phys.: Condens. Matter* **30** 283002
- [14] El-Barbary A A, Telling R H, Ewels C P, Heggie M I and Briddon P R 2003 *Phys. Rev. B* **68** 144107
- [15] Ma Y, Lehtinen P O, Foster A S and Nieminen R M 2004 *New J. Phys.* **6** 68
- [16] Lehtinen P O, Foster A S, Ma Y, Krasheninnikov A V and Nieminen R M 2004 *Phys. Rev. Lett.* **93** 187202
- [17] Yazyev O V and Helm L 2007 *Phys. Rev. B* **75** 125408
- [18] Casartelli M, Casolo S, Tantardini G F and Martinazzo R 2013 *Phys. Rev. B* **88** 195424
- [19] Palacios J J and Ynduráin F 2012 *Phys. Rev. B* **85** 245443
- [20] Wang B and Pantelides S T 2012 *Phys. Rev. B* **86** 165438
- [21] Rodrigo L, Pou P and Pérez R 2016 *Carbon* **103** 200–8
- [22] Valencia A M and Caldas M J 2017 *Phys. Rev. B* **96** 125431
- [23] Ronchi C, D'Atteo M, Perilli D, Ferrighi L, Fazio G, Selli D and Di Valentin C 2017 *J. Phys. Chem. C* **121** 8653–61
- [24] Casartelli M, Casolo S, Tantardini G F and Martinazzo R 2014 *Carbon* **77** 165–74
- [25] Anderson P W 1961 *Phys. Rev.* **124** 41–53
- [26] Levine R D 1969 *Quantum Mechanics of Molecular Rate Processes* (London: Oxford University Press)
- [27] Taylor J R 1969 *Scattering Theory: The Quantum Theory of Nonrelativistic Collisions* (Malabar, FL: Robert E. Krieger Publishing Company)
- [28] Wang Z F, Xiang R, Shi Q W, Yang J, Wang X, Hou J G and Chen J 2006 *Phys. Rev. B* **74** 125417
- [29] Sherafati M and Satpathy S 2011 *Phys. Rev. B* **83** 165425
- [30] Sherafati M and Satpathy S 2011 *Phys. Rev. B* **84** 125416
- [31] Kogan E 2011 *Phys. Rev. B* **84** 115119
- [32] Cheianov V V and Fal'ko V I 2006 *Phys. Rev. Lett.* **97** 226801
- [33] Mariani E, Glazman L I, Kamenev A and von Oppen F 2007 *Phys. Rev. B* **76** 165402
- [34] Bena C 2008 *Phys. Rev. Lett.* **100** 076601
- [35] Gonzalez-Herrero H, Gomez-Rodriguez J M, Mallet P, Moaied M, Palacios J J, Salgado C, Ugeda M M, Veuillen J Y, Yndurain F and Brihuega I 2016 *Science* **352** 437–41
- [36] Soler J M, Artacho E, Gale J D, García A, Junquera J, Ordeón P and Sánchez-Portal D 2002 *J. Phys.: Condens. Matter* **14** 2745
- [37] Artacho E *et al* 2008 *J. Phys.: Condens. Matter* **20** 064208
- [38] Kleinman L and Bylander D M 1982 *Phys. Rev. Lett.* **48** 1425–8
- [39] Troullier N and Martins J L 1991 *Phys. Rev. B* **43** 1993–2006
- [40] Louie S G, Froyen S and Cohen M L 1982 *Phys. Rev. B* **26** 1738–42
- [41] Zhang Y, Li S Y, Huang H, Li W T, Qiao J B, Wang W X, Yin L J, Bai K K, Duan W and He L 2016 *Phys. Rev. Lett.* **117** 166801
- [42] Martinazzo R 2023 *UNIMI Dataverse* (https://doi.org/10.13130/RD_UNIMI/EIMQRQ)